JCI insight

RESEARCH ARTICLE

Interspecies NASH disease activity whole-genome profiling identifies a fibrogenic role of PPARα-regulated dermatopontin

Philippe Lefebvre,[1] Fanny Lalloyer,[1] Eric Baugé,[1] Michal Pawlak,[1] Céline Gheeraert,[1] Hélène Dehondt,[1] Jonathan Vanhoutte,[1] Eloise Woitrain,[1] Nathalie Hennuyer,[1] Claire Mazuy,[1] Marie Bobowski-Gérard,[1] Francesco Paolo Zummo,[1] Bruno Derudas,[1] Ann Driessen,[2] Guy Hubens,[3] Luisa Vonghia,[4,5] Wilhelmus J. Kwanten,[4,6] Peter Michielsen,[4,6] Thomas Vanwolleghem,[4,6] Jérôme Eeckhoute,[1] An Verrijken,[5,6] Luc Van Gaal,[5,6] Sven Francque,[4,6] and Bart Staels[1]

[1]University Lille, Inserm, CHU-Lille, Institut Pasteur de Lille, U1011-EGID, Lille, France. [2]Department of Pathology, [3]Department of Abdominal Surgery, [4]Department of Gastroenterology and Hepatology, and [5]Department of Endocrinology, Diabetology and Metabolism, University Hospital Antwerp, Edegem, Belgium. [6]Laboratory of Experimental Medicine and Pediatrics, University of Antwerp, Antwerp, Belgium.

Nonalcoholic fatty liver disease prevalence is soaring with the obesity pandemic, but the pathogenic mechanisms leading to the progression toward active nonalcoholic steatohepatitis (NASH) and fibrosis, major causes of liver-related death, are poorly defined. To identify key components during the progression toward NASH and fibrosis, we investigated the liver transcriptome in a human cohort of NASH patients. The transition from histologically proven fatty liver to NASH and fibrosis was characterized by gene expression patterns that successively reflected altered functions in metabolism, inflammation, and epithelial-mesenchymal transition. A meta-analysis combining our and public human transcriptomic datasets with murine models of NASH and fibrosis defined a molecular signature characterizing NASH and fibrosis and evidencing abnormal inflammation and extracellular matrix (ECM) homeostasis. Dermatopontin expression was found increased in fibrosis, and reversal of fibrosis after gastric bypass correlated with decreased dermatopontin expression. Functional studies in mice identified an active role for dermatopontin in collagen deposition and fibrosis. PPARα activation lowered dermatopontin expression through a transrepressive mechanism affecting the Klf6/TGFβ1 pathway. Liver fibrotic histological damages are thus characterized by the deregulated expression of a restricted set of inflammation- and ECM-related genes. Among them, dermatopontin may be a valuable target to reverse the hepatic fibrotic process.

Introduction

Excessive, high-energy diets trigger a plethora of chronic pathologies, most of them remaining asymptomatic for many years until serious clinical complications occur. Among them, nonalcoholic fatty liver disease (NAFLD) is strongly associated with obesity and insulin resistance and predisposes patients to hepatic and extrahepatic disorders such as cirrhosis, type 2 diabetes, and cardiovascular diseases (1). NAFLD encompasses a broad spectrum of liver histological alterations, ranging from simple steatosis (NAFL) to hepatocyte cell death (ballooning) and inflammation (nonalcoholic steatohepatitis [NASH]). Although not a prerequisite for diagnosis, fibrosis can also occur (2) and is an indicator of liver-related mortality risk in NAFLD patients (3).

Highly related to wound-healing processes, fibrosis is the result of an exacerbated but reversible response leading to both qualitatively and quantitatively abnormal extracellular matrix (ECM) deposition (4). ECM homeostasis in the liver depends on the orchestrated interplay of hepatic stellate cells (HSCs) with other cells such as parenchymal and liver sinusoidal endothelial cells (LSECs), which regulate ECM deposition and resorption (5). These processes are under the control of autocrine and paracrine signals, such as the TGFβ, PDGF, connective tissue growth factor (CTGF), and Hippo pathways (6, 7), and ensure optimal tissue functionality owing to the mechanical and biochemical properties of ECM.

Authorship note: SF and BS are co–senior authors.

Conflict of interest: BS and SF are consultants for Genfit SA.

Submitted: December 15, 2016
Accepted: May 19, 2017
Published: July 6, 2017

Reference information:
JCI Insight. 2017;2(13):e92264.
https://doi.org/10.1172/jci.insight.92264.

In NASH, iterative deleterious signals activate LSECs and HSCs (8, 9), thereby compromising ECM component production and turnover. The ensuing fibrotic process functionally and structurally alters the intrahepatic vasculature, and a complex cascade of events can ultimately lead to cirrhosis and its complications, including increased death rates (10, 11). Active NASH with fibrosis is therefore a major risk factor in NAFLD-related morbidity and mortality.

Loss of body weight improves the histological features of NAFLD (12). This can be achieved by lifestyle modification, but most patients fail to reach the required goals to achieve reversal of the disease (12). Bariatric surgery (BarSur) is the most effective procedure to induce sustained weight loss and triggers profound positive metabolic effects in obese and diabetic patients. It also is highly effective to reverse NASH and fibrosis in obese patients (13–17). Although there are no pharmacological options for the treatment of NASH or fibrosis, a few potentially valuable molecules are currently under clinical evaluation. For example, activation of the PPAR nuclear receptors in preclinical models protects from dietary-induced or genetically induced NASH and fibrosis (18, 19). Assessment of the translation of such observations to human pathology is currently underway. These yet-unmet clinical needs therefore call for the identification of the protagonists of NASH and fibrosis.

Mechanistic, preclinical, and clinical studies delineated molecular pathways contributing to the progression of NAFLD from NAFL to NASH and fibrosis (20, 21). Gene profiling experiments in cross-sectional studies have proven useful in identifying factors involved in NAFLD progression. Performed on cohorts stratified on the basis of more or less refined histological parameters (alcoholic steatohepatitis and NASH vs. no NASH, NASH vs. no NASH, control vs. steatosis vs. NASH, control vs. steatosis vs. NASH with steatosis > 5% vs. NASH with steatosis < 5%; refs. 22–26), these studies identified specific protagonists such as the Wnt pathway; genes involved in absorption, distribution, metabolism, and excretion (ADME); aldose reductase *AKR1B10*; and keratin family member *KRT23*. Comparing the liver transcriptome of NAFLD patients with no or little fibrosis to the one of fibrotic patients revealed genes involved in cellular proliferation and ECM organization (27, 28).

Meta-analysis is a robust method to define disease molecular signatures and to identify potential biomarkers (29). We therefore undertook a transcriptomic study of liver biopsies from 87 nondiabetic overweight/obese patients, which were metabolically and histologically phenotyped and represented all stages of NAFLD and fibrosis progression. A meta-analysis of our and publicly available datasets with comparable histological features was carried out to identify genes that are dysregulated in NASH and fibrosis. As gastric bypass (GABY) is most efficient to induce improvement of NAFLD, a paired analysis of the liver transcriptome before GABY and after a 1-year follow-up was used to identify genes whose expression is normalized by this surgical procedure, indicating their potential role in the pathophysiology of the disease and its resolution. Data were further crossed with transcriptomic data from NASH and fibrosis mouse models. Together with gene ontology (GO) classification, gene set enrichment analysis (GSEA), and other data-mining strategies, we identified a conserved set of genes, many of which associated to ECM homeostasis. Among them, dermatopontin (*DPT*) was upregulated in active NASH and fibrosis. It was further characterized since *Dpt* encodes a protein controlling skin collagen fibrillogenesis (30) through interaction with fibronectin (31–33), and it interacts with TGFβ (34). *Dpt* expression was found to be necessary for collagen deposition in profibrotic conditions and was normalized by GABY in humans and by PPARα activation in mice through a transrepression mechanism.

Results

Transcriptomic analysis of liver biopsies from overweight patients with different degrees of NASH and fibrosis. Transcriptomic analysis of 87 liver biopsies from patients with distinct degrees of metabolic alterations, inflammation, and fibrosis (Table 1) was performed to identify transcripts coding for proteins that exhibit a > 20% differential expression level across samples, a threshold below which technical variation precludes reliable detection of gene expression variation. This defined a restricted set of 6,925 protein-encoding genes whose expression could be clustered through a self-organizing map (SOM) (Supplemental Figure 1A and Supplemental Table 1; supplemental material available online with this article; https://doi.org/10.1172/jci.insight.92264DS1). GO term enrichment of gene clusters pointed at pathways known to be altered in liver diseases (Supplemental Figure 1B and Supplemental Table 1), such as ECM deposition, immune response, regulation of transcription, and nuclear receptors, including the PPARα pathway recently shown to be involved in liver inflammation and fibrosis in humans and rodents (35, 36). However, this unsupervised

Table 1. Patient clinical and biochemical characteristics

	Mean ± SEM[A]	(Min/max)
Age	45.55 ± 12.81	(20–74)
BMI (kg/m²)	38.91 ± 5.99	(27–69)
Total cholesterol (mg/dl)	202 ± 37	(118–295)
HDL cholesterol (mg/dl)	46 ± 13	(24–102)
Triglycerides (mg/dl)	168 ± 97	(45–675)
LDL cholesterol (mg/dl)	122 ± 31	(49–212)
HbA1C (%)	5.61 ± 0.64	(4–10.2)
Fasting glucose (mg/dl)	4.79 ± 0.87	(3.4–10.7)
CRP (ng/ml)	0.67 ± 0.69	(0.03–4.55)
Steatosis (0:1:2:3)	11:30:24:22	
Ballooning (0:1:2)	18:39:30	
Lobular inflammation (0:1:2:3:4)	16:51:32:4	
NAS score (0–8)	8:3:9:11:26:7:16:6:1	
Fibrosis stage (0:1:2:3:4)	54:20:7:5:1	

[A]*n* = 87 (55 females, 32 males). Results are expressed as the mean ± SEM. The lower and upper values are indicated (Min/max). Numbers in the right column (x:y:z) indicate the distribution of patients according to the histological criteria. HDL, high-density lipoprotein; LDL, low-density lipoprotein; CRP, C-reactive protein; NAS score, NAFLD activity score.

learning–based clustering strategy did not yield a clear-cut patient grouping according to biological or histological parameters, probably reflecting the diverse biological status of patients at the time of biopsy.

Expressing hepatic gene expression variation as a function of quantified biological or histological parameters was therefore used as an alternative method. To do so, we analyzed, in a pair-wise manner, gene expression data from patients displaying no sign of alteration vs. those from patients with pronounced alteration of a given parameter (Supplemental Figure 2). This analysis was coupled to a GO term enrichment analysis to avoid any bias in selecting biological pathways emerging from the differential gene expression analysis. We first compared gene expression patterns of groups of patients with markedly different biometric (BMI) or systemic metabolic parameters (total cholesterol, triglycerides, homeostatic model assessment of insulin resistance (HOMA-IR). This analysis provided no evidence for a global alteration of genes involved in these systemic metabolic functions (Supplemental Table 2), although a stratification based on BMI or HOMA-IR identified genes involved in lipid metabolism and reported to be dysregulated in NAFLD/NASH (*FASD1* and *FASD2*, *NR0B2* and *ELOVL2*; refs. 22, 24). In contrast, comparison of the liver transcriptomes from patients displaying different stages of hepatic histological damages with controls clearly identified functionally related clusters of genes. This approach was applied to steatosis, to the combination of lobular inflammation and ballooning, and to fibrosis. For example, a high fibrosis stage (F2–4 vs. F0) correlated with an upregulated expression of genes involved in the immune response and ECM remodeling, including collagen fibril organization (*COL1A1*, *COL1A2*, *COL3A3*, *COL14A1*, *DPT*, *LUM*) and HSC activation (*TGFB1*) (Supplemental Figure 3, A and B; and Supplemental Table 2). In contrast, repressed genes in fibrotic livers were related to metabolic processes (Supplemental Figure 3B). This comparative analysis for steatosis, for lobular inflammation and ballooning, and for fibrosis highlighted a progressive shift from metabolic disturbances in NAFL/steatosis to inflammatory responses in active NASH and ECM remodeling in fibrosis, evidenced by the altered expression of 251 genes in total (Figure 1A).

As necroinflammation and ballooning are the hallmark of NASH (20, 37), we generated gene lists containing all up- and downregulated genes in lobular inflammation (grade ≥ 2) and ballooning (grade > 1), which correspond to the current concept of definite or moderate-to-severe NASH. This list was combined with that of genes dysregulated in fibrosis (≥F2) to generate a gene signature corresponding to a "definite NASH + fibrosis" state (Supplemental Table 3). As expected, functional annotation of the upregulated gene list (193 genes) very significantly identified molecular functions related to immune responses and ECM homeostasis, whereas metabolic processes were predominantly identified in the downregulated 58-gene set (data not shown).

Weight loss by BarSur induced liver lesion regression, whereas lifestyle modification resulted in little improvement. We therefore restricted the paired biopsy analysis to patients who, after their initial work-up, went to GABY. BarSur has been previously shown to efficiently normalize biochemical parameters and reverse liver pathological features (13–16). The positive effect of GABY on biological constants and on liver histological features was also observed in our cohort

Table 2. Effects of bariatric surgery in obese patients

	Bariatric surgery		
	M_0	M_{12}	*P* value
BMI	40.20 ± 4.40	28.62 ± 5.71	2.5×10^{-10}
IGF-1	164.60 ± 52.30	170.17 ± 62.24	7.4×10^{-01}
Chol	219.20 ± 61.50	172.90 ± 41.77	2.8×10^{-03}
HDL	49.00 ± 15.80	56.24 ± 16.11	1.1×10^{-01}
LDL	137.90 ± 54.70	94.38 ± 31.26	1.1×10^{-03}
TG	161.80 ± 72.20	104.70 ± 38.32	9.9×10^{-04}
Glucose	85.50 ± 14.10	76.04 ± 15.76	3.1×10^{-02}
Insulin	17.70 ± 9.60	7.67 ± 3.82	9.8×10^{-06}
C Peptide	1.20 ± 0.40	0.82 ± 0.49	5.7×10^{-03}
HbA1c	5.70 ± 0.51	5.03 ± 0.98	3.7×10^{-03}
HOMA-IR	3.90 ± 2.51	1.50 ± 0.77	2.4×10^{-05}

Clinical and biochemical parameters of patients before and after bariatric surgery. BMI (kg/m²); Chol., cholesterol (mg/dl); HDL, high-density lipoprotein (mg/dl); LDL, low-density lipoprotein (mg/dl); TG, triglycerides (mg/dl); CRP, C-reactive protein (mg/l); IGF-1, insulin-like growth factor-1 (ng/l).

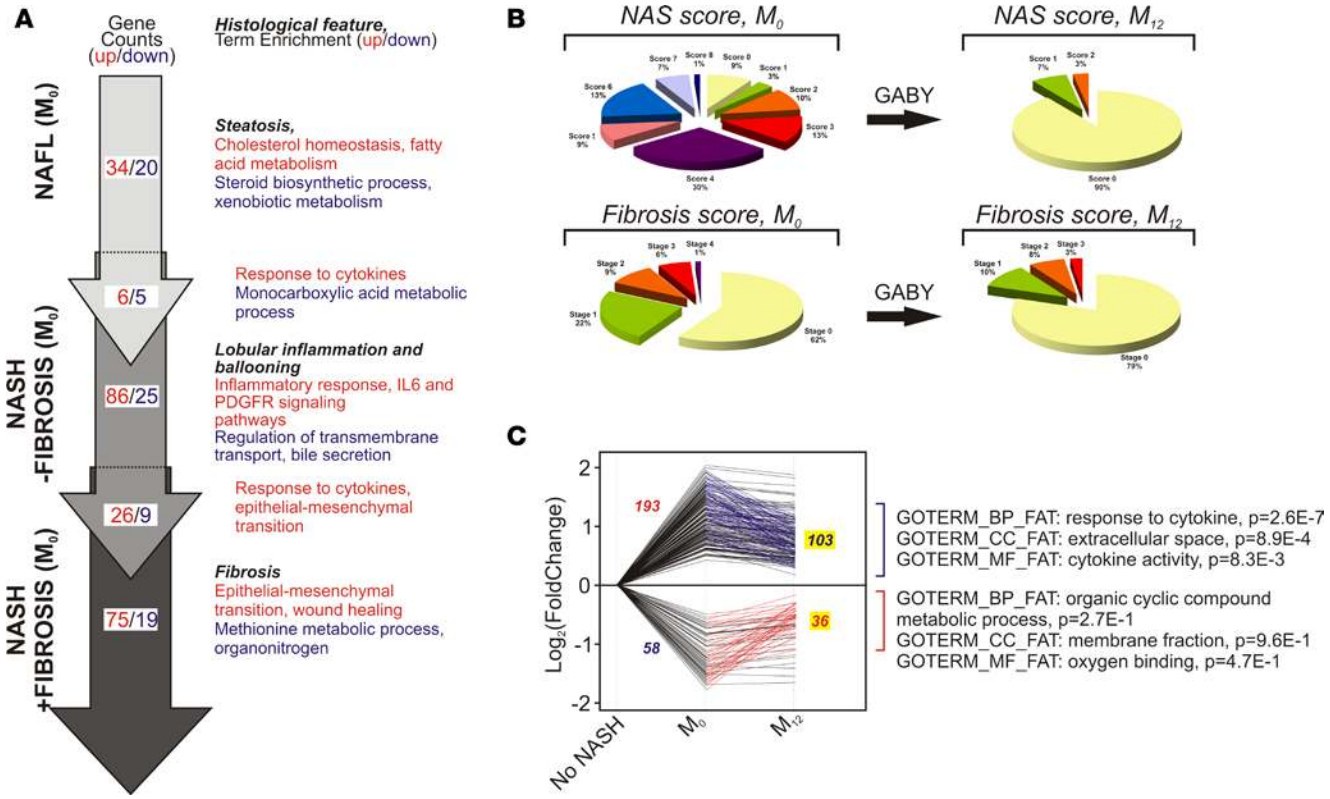

Figure 1. Gene expression patterns in NAFLD and fibrosis progression and regression upon GABY. (**A**) The cohort was stratified in 3 categories (nonalcoholic fatty liver, NAFL), nonalcoholic steatohepatitis (NASH) without fibrosis (NASH – fibrosis), and NASH with fibrosis (NASH + fibrosis). Differentially expressed genes were identified as described in Supplemental Table 3 and Supplemental Figure 3 (red, upregulated; blue, downregulated) by comparing gene expression patterns of patients displaying no sign of alteration vs. those from patients with pronounced alteration of a given parameter (see Supplemental Figure 2). Gene lists were annotated with the gene ontology (GO) biological process functional annotation table, and resulting biological term enrichment are shown. (**B**) Evolution of the NAS score and of fibrosis after gastric bypass (GABY). (**B**) Patient stratification according to histological parameters. Patients were histologically graded and classified according to the NAS score, lobular inflammation, or fibrosis stages prior to surgery (M_0) or 1 year after intervention (M_{12}). (**C**) Genes whose expression was either up- or downregulated in lobular inflammation, ballooning, or fibrosis were selected to build 2 gene lists that are either up- or downregulated in the 3 categories (193 and 58 genes respectively, 2-tailed *t* test, FC > 1.2, $P < 0.05$). These gene lists were crossed with those containing genes showing an inverse regulation after GABY. Green lines indicate the 103 genes upregulated in either lobular inflammation, ballooning, or fibrosis whose expression is decreased after GABY. Red lines indicate the 36 genes downregulated in either lobular inflammation, ballooning, or fibrosis whose expression is increased after GABY. Gene expression values are expressed relative to normalized control values (no lobular inflammation, ballooning, or fibrosis) arbitrarily set to 1 and expressed as $\log_2$ fold change. (Right) Top ranking hits after a GO term enrichment analysis (Metascape) against biological process (BP), cellular components (CC), or molecular functions (MF) functional annotation tables (FAT) are indicated.

(Table 2 and Figure 1B, respectively). Indeed, GABY induced a general regression of the NAFLD activity score (NAS score) and of the fibrosis stage (Figure 1B), which correlated with a global downregulation of genes functionally not only associated to the immune and inflammatory response, but also to extracellular space/matrix homeostasis (Supplemental Figure 4 and Supplemental Tables 4, 5, 6). Thus, human NASH and fibrosis induce a transcriptional program strongly related to inflammation and ECM remodeling, processes that can be reversed by GABY.

To identify the genes associated with increased NAFLD/NASH and fibrosis stages (Figure 1A) and whose expression can be reverted upon improvement of liver histological parameters by GABY, we assessed the regulation of the 193 upregulated and 58 downregulated genes in the "NASH – fibrosis" or "NASH + fibrosis" state before (M_0) or after GABY (M_{12}) (Figure 1C and Supplemental Table 6). The expression of > 50% of these 251 genes was partially or totally normalized after GABY (M_{12}: upregulated genes, 103/193; and downregulated genes, 36/58), many of them participating in immune responses and ECM deposition (*THBS1*/thrombospondin, *CLEC7A*/*dectin1*, *IL18*, chemokine CC and CXC ligands) as shown by GO term enrichment analysis (Figure 1C). Thus, our transcriptomic analysis identified a limited set of 139 human genes with functions in inflammation and ECM remodeling whose expression changes in NASH or NASH + fibrosis and is normalized by GABY.

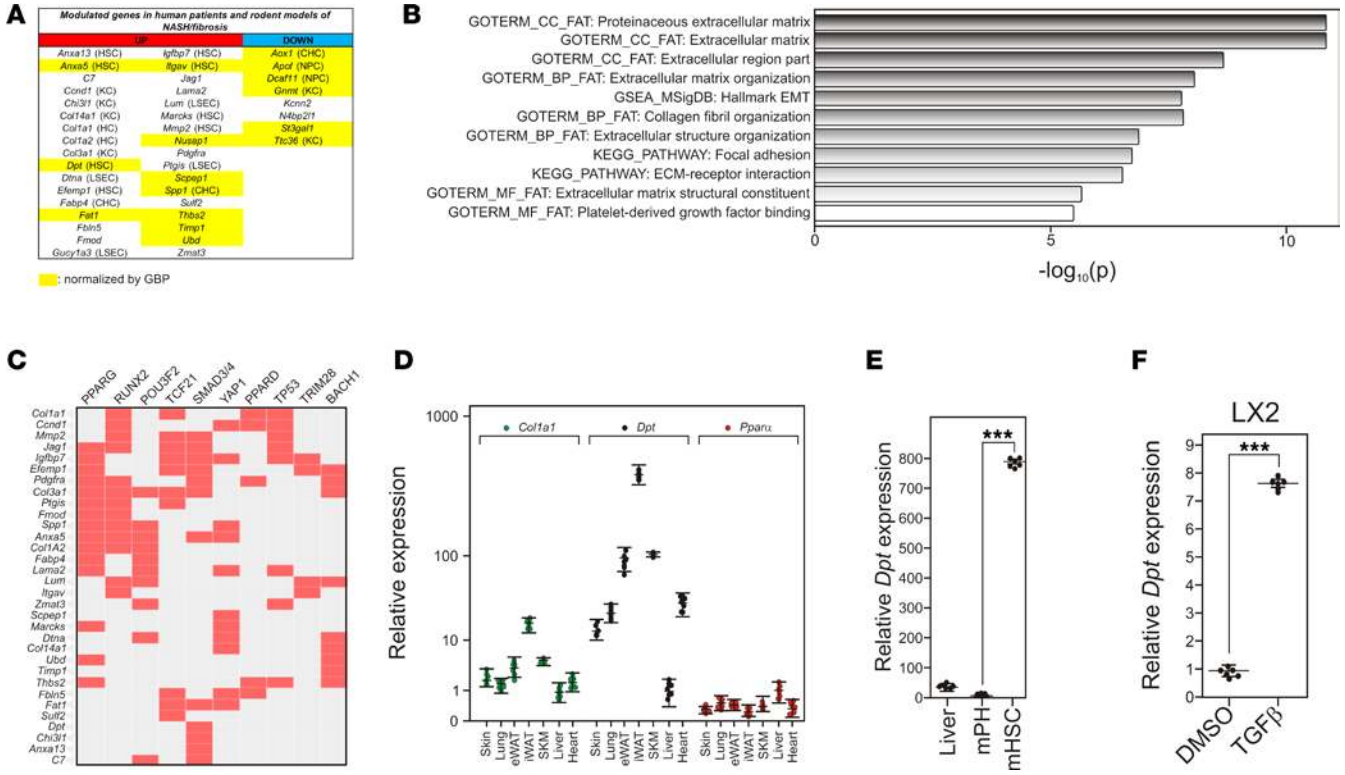

Figure 2. Identifying *dermatopontin* as a potential contributor to liver fibrosis. (**A**) Up- and downregulated genes in mouse models of nonalcoholic steatohepatitis (NASH) or fibrosis and in human cohorts of NASH + fibrosis patients. Gene symbols are indicated in each column. Cell type–specific expression is indicated when known (HSC, hepatic stellate cell; KC, Kuppfer cell; HC: hepatocyte; LSEC, liver sinusoidal endothelial cell; CHC, intrahepatic cholangiocyte; NPC, nonparenchymal cell). A complete list of genes can be found in Supplemental Table 10. Genes whose expression is normalized by gastric bypass (GABY) are highlighted in yellow. (**B**) Top-ranking terms characterizing upregulated genes in advanced NASH. The upregulated gene list was searched against the Hallmark gene sets, gene ontology (GO) biological processes, GO cellular components, and GO molecular functions annotation table, as well as the KEGG pathway database using Metascape. (**C**) Potential regulatory pathways. The upregulated gene list was scanned for the occurrence of actual transcription factor binding site as determined by ChIP-Seq assays from the ENCODE and ChEA databases using the EnrichR web server (http://amp.pharm.mssm.edu/Enrichr/) (82, 83). Positive hits are indicated in red. (**D**) Tissue-specific expression of *Dpt* in mouse tissues. RNAs were extracted from indicated tissues and analyzed by qPCR. Results are expressed relative to a control value arbitrarily set to 1 (liver) and are the mean ± SEM (n = 6). Data were compared using a 2-tailed ANOVA corrected for multiple comparisons using the Dunnett's post hoc test. ***$P < 0.005$. (**E**) Relative expression of *Dpt* in mouse purified hepatocytes and hepatic stellate cells. (**F**) Relative expression of *DPT* in TGFβ-stimulated (10 ng/ml, 24 hours) LX2 cells.

To make a more stringent selection of genes involved in NASH and fibrosis progression, we assessed which genes dysregulated in our cohort could be validated in other human cohorts. Therefore, two transcriptomic studies were selected (24, 27) to which similar filters (inflammation ≥ 2, fibrosis ≥ F2) and analysis methods were applied. A comparison of differentially expressed genes in all 3 cohorts, which showed similarly dysregulated biological processes (Supplemental Figure 5), generated a human NASH + fibrosis core signature containing 48 upregulated and 10 downregulated genes (Supplemental Figure 6 and Supplemental Table 7), the former being strongly enriched in genes involved in ECM formation (*COL1A1* and *-2*, *COL3A1*, *COL14A1*, *DPT*, *FBLN5*, *LUM*, *PDGFRA*) and inflammatory responses (*CCL19* and *-21*, *CXCL9* and *-10*, *SPP1*) (Supplemental Figure 6). Very interestingly, the expression of 24 of these 58 genes was normalized after GABY in our cohort, thereby identifying GABY-sensitive human genes with potential pathogenic activity (Supplemental Figure 6).

Transcriptional alterations in rodent models of NASH and fibrosis. Conserved cross-species regulatory mechanisms are strongly indicative of shared biological functions. We therefore carried out a transcriptomic meta-analysis of several murine preclinical models that mimic certain aspects of human liver pathology (38). Feeding mice a methionine and choline-deficient diet (MCDD) promotes pathological features typical of liver inflammation and early fibrosis without inducing systemic metabolic alterations of human NASH. MCDD has been used in combination with a high-fat diet (HFD) to install NASH in a context of insulin resistance. Although there is no well-established, reproducible model of dietary-induced fibrosis, fibrosis can

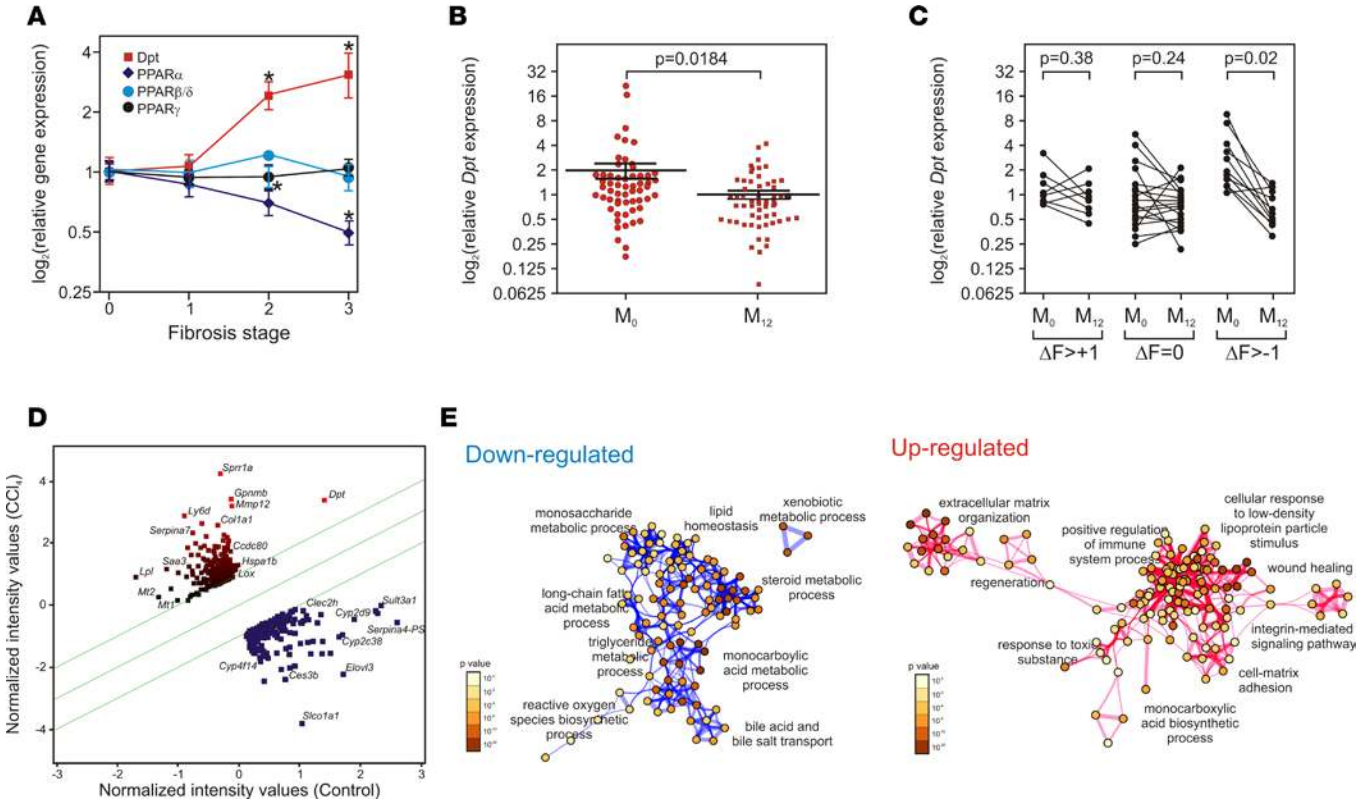

Figure 3. *DPT* expression correlates with human fibrosis severity. (**A**) Human *DPT* and *PPAR* expression as a function of the fibrosis stage. *PPARα*, *PPARβ/δ*, and *PPARγ* expression levels were extracted from microarray data and expressed relative to control (no fibrosis) arbitrarily set to 1. Expression values are expressed as the mean ± SEM (n = 16–35) and compared using a 2-tailed ANOVA corrected for multiple comparisons using the Dunnett's post hoc test. *$P < 0.05$. (**B**) *DPT* mRNA expression level after gastric bypass (GABY). *DPT* expression level were assayed by qPCR and expressed relative to a randomly chosen baseline value set to 1. Data are expressed as the mean ± SEM and were compared using an unpaired t test (n = 52). (**C**) Correlation between fibrosis evolution and *DPT* expression in human fibrotic livers. *DPT* expression was plotted before (M_0) and after GABY (M_{12}) as a function of the fibrosis-stage evolution. Expression values, assayed by qPCR, were compared using a paired t test. (**D**) Scatter plot of differentially expressed genes in carbon tetrachloride–treated (CCl_4-treated) $Dpt^{+/+}$ mice. Gene expression was assayed using Affymetrix array (n = 6) and analyzed using the Genespring 14.3 software. Upregulated genes are indicated in red, downregulated genes in green. The fold change (FC) threshold was set at 2 ($P < 0.05$) and is indicated by the two green lines. The most relevant gene symbols are indicated; a complete listing of induced and repressed genes can be found in supplemental Table 9. *Dpt* was induced 4-fold. (**E**) Up- and downregulated gene lists underwent a gene ontology (GO) term enrichment against the biological process function annotation table (Metascape, settings: minimum overlap 5, P value cutoff 0.01, minimum enrichment 5). Statistically enriched terms were converted into a network layout in which circle diameters are proportional to the number of genes and the thickness of edges indicates the similarity score. The color scales indicate the P value of the nodes. A complete list of genes can be found in supplemental Table 11.

be chemically induced by carbon tetrachloride (CCl_4), which induces oxidative damages through conversion of CCl_4 to the trichloromethyl radical ·CCl3 by Cyp2E1, a pericentral hepatocyte-specific enzyme (39, 40).

We next evaluated whether the human transcriptomic signatures associated with pathological features of NASH are recapitulated in mice fed a HFD/MCDD. Gene expression changes (Supplemental Table 8) were functionally related to inflammatory cell migration, lipid metabolism, responses to TGFβ and extracellular matrix organization (upregulated genes), and amino acid and bile acid metabolism (downregulated genes) (Supplemental Figure 7). We similarly assessed if HFD feeding combined with CCl_4 reproduced part of the transcriptional alterations observed in human fibrosis. HFD/CCl_4 treatment massively downregulated numerous cytochrome P450 genes, paralleling a strong upregulation of chemokines involved in chemotaxis and enzymes participating in ECM formation (Supplemental Figure 8 and Supplemental Table 9), patterns resembling part of the functional programs induced in human fibrosis.

Combining the dysregulated gene sets in the MCD/HF and CCl_4/HF diet models defined a set of genes characterizing the liver response to experimentally induced NASH or fibrosis, respectively. By comparing the human GABY-sensitive 139-gene list to this murine gene repertoire, we generated a conserved core gene signature of 34 upregulated genes and 8 downregulated genes for NASH + fibrosis (Figure 2A and Supplemental Table 10). Quite strikingly, GSEA and GO enrichment analysis of the 34 upregulated genes pointed to

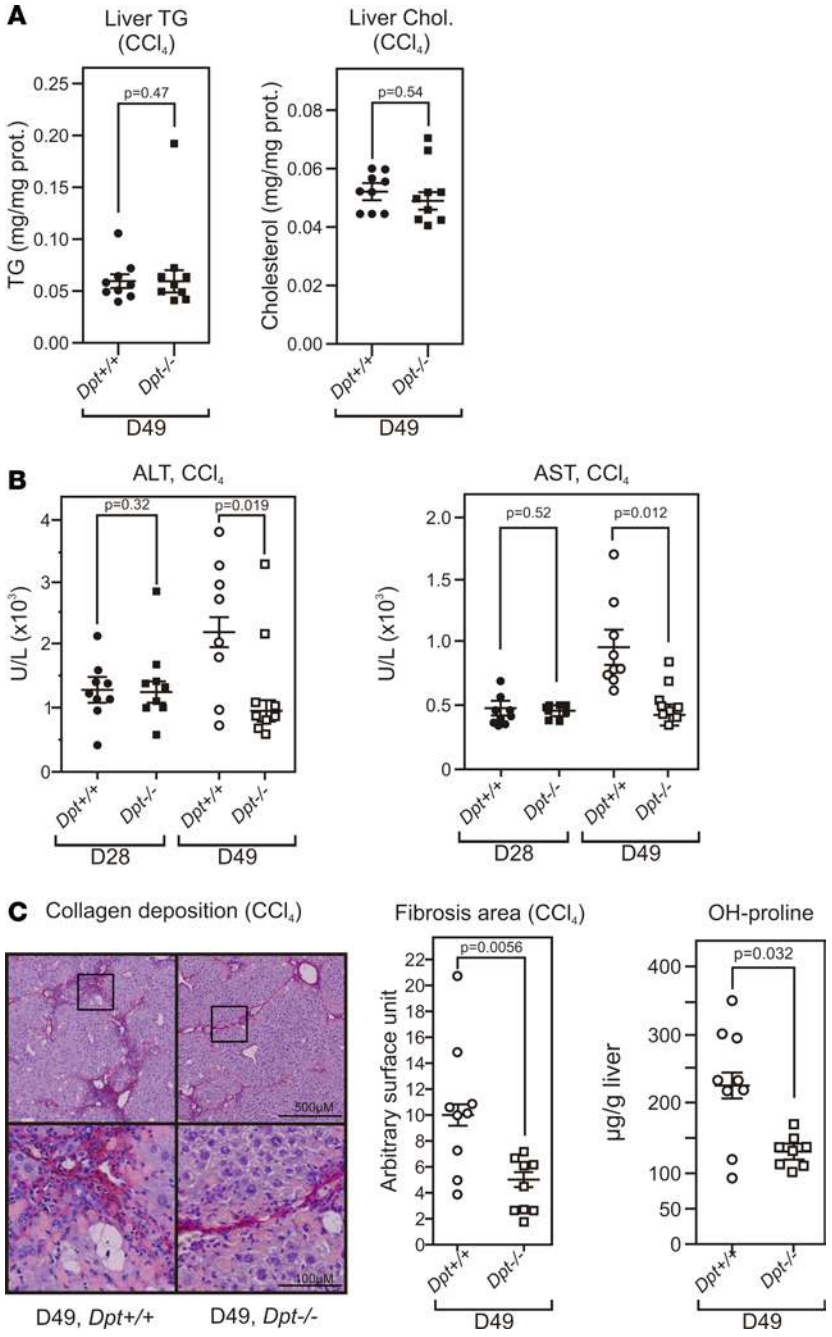

Figure 4. Dermatopontin is a critical player in the chemically induced fibrotic response. (**A**) Hepatic triglyceride and cholesterol content in Dpt$^{-/-}$ mice. Hepatic triglycerides (TG) content was assayed in CCl_4-treated WT (*Dpt*$^{+/+}$, *n* = 9) and Dpt-null mice (*Dpt*$^{-/-}$, *n* = 8). Data are expressed as the mean ± SEM (*n* = 8–9) of mg TG per mg liver protein and were compared using a 2-tailed *t* test. The *P* value is indicated. Hepatic cholesterol content was assayed in WT (*Dpt*$^{+/+}$, *n* = 9) and *Dpt*-null mice (*Dpt*$^{-/-}$, *n* = 8). Data are expressed as mg TG per mg liver protein and were compared using a 2-tailed *t* test. The *P* value is indicated. (**B**) Alanine aminotransferase (ALT) and aspartate aminotransferase (AST) plasma level in CCl_4-treated WT or *Dpt*$^{-/-}$ mice. Mice (*n* = 9) were treated biweekly for the indicated period (28 or 49 days) with CCl_4, and liver enzymes were assayed as described (36). Data are expressed as the mean ± SEM of enzymatic units/L (U/l) and were compared using a 2-tailed *t* test (*n* = 8–9). The *P* value is indicated. (**C**) Hepatic collagen deposition in CCl_4-treated *Dpt*$^{+/+}$ or *Dpt*-KO mice treated for 49 days with CCl_4. Paraffin-embedded liver sections were stained with Sirius red, and the collagen deposition area was quantified with the ImageJ software. Data are expressed as the percentage of the total area and were compared using a 2-tailed Mann Whitney test. *P* value is indicated. The liver collagen content was measured using a hydroxyproline assay. Results are expressed as the mean ± SEM of µg hydroxyproline per g liver and were compared using a 2-tailed *t* test. The *P* value is indicated.

functions in epithelial mesenchymal transition and ECM deposition (Figure 2B), processes likely to occur simultaneously upon HSC dedifferentiation and fibrogenesis. This conclusion was supported by filtering this list of 34 upregulated genes against ChIP-X databases, showing that their upstream regulatory regions contain bona fide binding sites for PPARs and/or RunX2 and/or Smad transcription factors (Figure 2C), all involved in HSC responses to liver injury (41). Of note, 20 of the 34 upregulated genes display cell-specific expression in normal mouse liver, 8 of them being strongly expressed in HSCs (Figure 2A; refs. 42, 43).

The potential of these genes for human therapeutic intervention and clinical relevance was further assessed by identifying within this 42-gene list those sensitive to GABY, resulting in a 16-gene set (Figure 2A) whose properties (dysregulated in human and mouse NASH + fibrosis and normalized by GABY) indicate that they could be potential targets to reverse NASH and fibrosis progression.

DPT expression correlates with human fibrosis. Many of the upregulated genes have already been associated with ECM homeostasis and liver fibrosis, such as *Col14a1/undulin* (44), *Col1a1*, *Col1a2*, and *Col3a1*, as well as *Timp1* (45), *Lama2* (46), and *Lumican/Lum* (47). In contrast, the role of *Dpt* in hepatic pathophysiology is unknown. Previous reports hinted at a possible role of *Dpt* in dermis ECM homeostasis through an interaction of DPT with fibrin and fibrinogen (31, 33, 47, 48). The tissue-specific distribution of *Dpt* was assessed in several mouse tissues (Figure 2D), showing a predominant expression in adipose tissues, skin, and lungs, as previously reported in tissue atlas expression studies (http://biogps.org/#goto=genereport&id=1805). *Dpt* expression in the liver was low but detectable, but was strongly enriched (more than 800-fold) in purified HSCS (Figure 2E), in line with proteomic and RNA-seq data (42, 43). In agreement with our predictions (Figure 2C), *Dpt* expression was inducible by TGFβ in the human stellate LX2 cell line (Figure 2F).

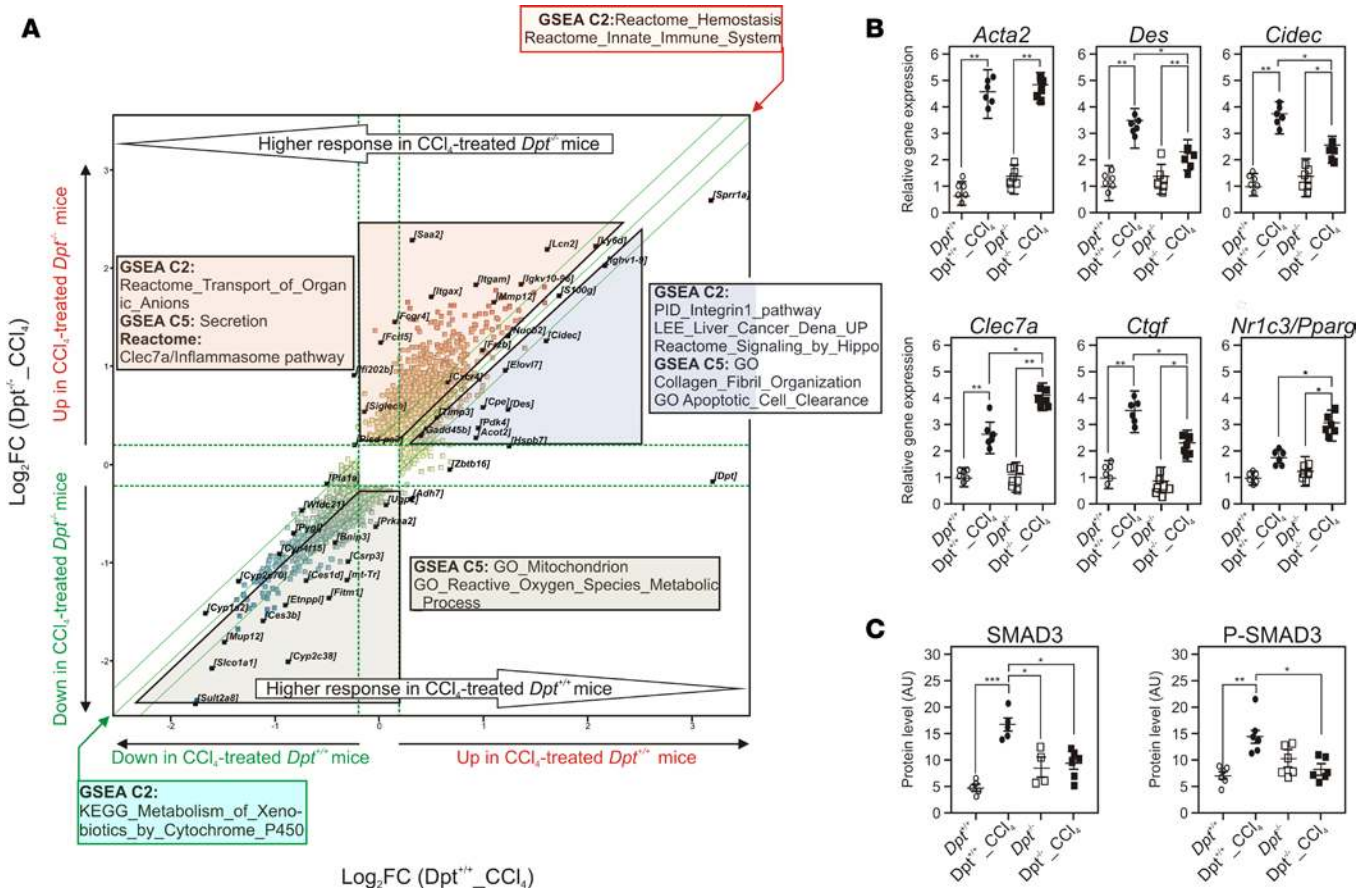

Figure 5. Dpt$^{-/-}$ mice display an altered response to CCl$_4$-induced injury. (**A**) The expression of hepatic genes was monitored using Affymetrix microarrays after RNA extraction from CCl$_4$-treated *Dpt*$^{+/+}$ or Dpt$^{-/-}$ mouse livers (n = 6). Gene expression patterns were compared using an unpaired t test (FC > 2, P < 0.05) and are shown as a scatter plot. Differentially expressed gene lists were analyzed by gene set enrichment analysis (GSEA); top-ranking gene sets are indicated. The two most extreme green lines indicate a fold change of 1.2. (**B**) Gene expression values for fibrosis-related genes. Normalized gene expression values were extracted from microarray data and were expressed relative to expression levels detected in unchallenged *Dpt*$^{+/+}$ mouse livers. (**C**) SMAD3 and phospho-SMAD3 protein levels. Quantification of protein levels after WES-based analysis (Supplemental Figure 10) are shown. Results are expressed as the mean ± SEM of densitometric arbitrary units (n = 6–8). Data were compared using a 2-tailed ANOVA corrected for multiple comparisons using the Dunnett's post hoc test. *P < 0.05, **P < 0.01, ***P < 0.005.

These observations, thus, raise the possibility that *Dpt* could participate in the hepatic fibrotic process, as HSCs are strongly involved in this process (49).

Expressing *DPT* expression as a function of human liver histological parameters (NAS score, fibrosis stage) indicated a positive correlation of *DPT* expression with fibrosis but not with the composite NAS score integrating steatosis, lobular inflammation, and ballooning stages (Supplemental Figure 9 and Figure 3A). Furthermore, *DPT* expression decreased after GABY (Figure 3B), and a paired analysis of fibrosis evolution after GABY revealed a significant decrease in *DPT* expression upon fibrosis regression by > 1 grade (Figure 3C). Thus, *DPT* expression is significantly associated with the fibrosis stage in human liver disease.

We next assessed whether the CCl$_4$-induced fibrosis model, which generates pericentral hepatocyte-specific oxidative stress, recapitulates features of human fibrosis. Four-hundred and ninety genes (fold cgange [FC] > 2, P < 0.05, Supplemental Table 11) were dysregulated in CCl$_4$-treated WT mice, which were highly similar to those induced by HFD/CCl$_4$ treatment (Supplemental Figure 8). A robust induction of the expression of *Dpt* (FC = 4), together with other genes related to ECM organization, was observed, whereas downregulated genes were mostly involved in metabolic processes (Figure 3, D and E). Interestingly, the fibrosis modulator gene expression pattern in the CCl$_4$ model resembled the one found in our human cohort, including increased expression of *Tgfb*, *Ctgf*, and *Pdgfb* (Supplemental Table 12). Taking together, these data validate the CCl$_4$-induced fibrosis model as a surrogate model for functional studies of genes identified in human fibrosis. We thus investigated whether *Dpt* modifies fibrosis development using this model.

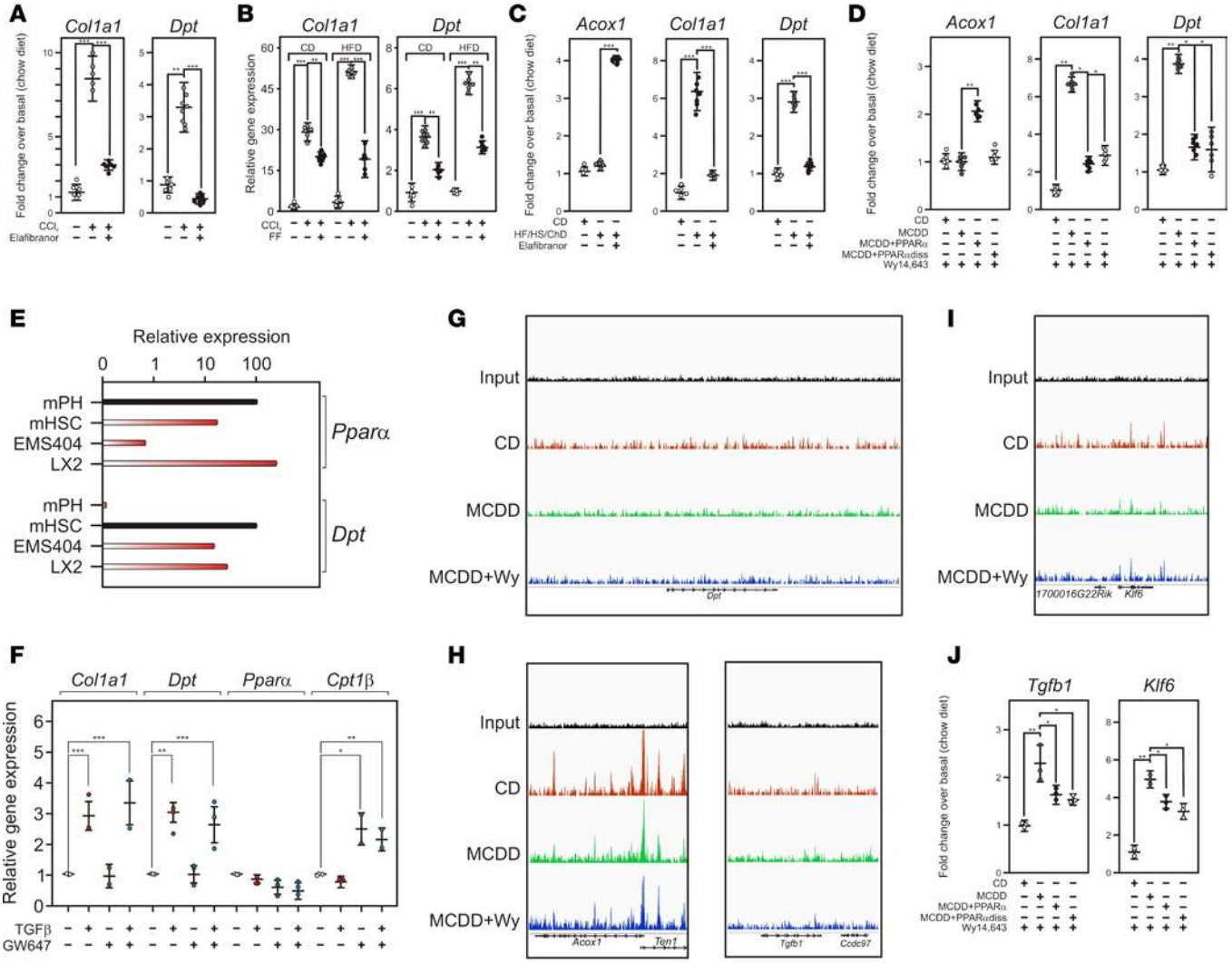

Figure 6. PPARα activation regulates *Dpt* expression. (**A**) Mouse *Dpt* gene regulation by PPARα/δ agonism. Mice were submitted to CCl_4 exposure and treated or not with elafibranor/GFT505. Gene expression was monitored by qPCR. Results are expressed relative to a control value arbitrarily set to 1 and are the mean ± SEM (n = 4–8). Data were compared as above. $^{**}P < 0.01$, $^{***}P < 0.005$. (**B**) Mouse *Dpt* gene regulation by PPARα agonism. Mice were fed either a normal chow (CD) or a high-fat diet (HFD) and submitted to CCl_4 exposure and treated or not with fenofibrate (200 mpk/day). Gene expression was monitored by qPCR. Results are expressed relative to a control value arbitrarily set to 1 and are the mean ± SEM (n = 5–8). Data were compared as above. $^{**}P < 0.01$, $^{***}P < 0.005$. Data were compared using a 2-tailed ANOVA corrected for multiple comparisons using the Dunnett's post hoc test. (**C**) *Dpt* regulation in a diet-induced model of NASH. Mice were fed a high-sucrose, HFD supplemented with 0.5% cholesterol and treated or not by elafibranor. Results were obtained and processed as in **A** (n = 8). (**D**) Mouse *Dpt* gene regulation by hepatic PPARα. Fourteen-week-old PPARα-KO mice (n = 11) were transduced with AAV8-TBG-PPARα viral particles (PPARα) or AAV8-TBG-PPARαdiss or not and were fed 2 weeks later a chow diet (CD) or a methionine and choline deficient diet (MCDD) for 3 weeks. Diets were then supplemented with 0.2% Wy14,643, a synthetic PPARα agonist, for 5 days. RNAs were extracted and analyzed by RT-PCR as described (36). Results are expressed relative to a control value arbitrarily set to 1 (CD) and are the mean ± SEM (n = 7). Data were compared using a 2-tailed ANOVA corrected for multiple comparisons using the Dunnett's post hoc test. $^{*}P < 0.05$, $^{**}P < 0.01$. (**E**) Relative expression of *Dpt* and *PPARα* in liver cells and cell lines. Transcript abundance was assayed by qPCR (n = 3) and expressed relative to highest expressing cells arbitrarily set to 100 (black bars). mPH, mouse primary hepatocytes; mHSC, mouse primary hepatic stellate cells. (**F**) Relative expression of genes in TGFβ1-treated cells. mRNAs were quantified by qPCR and expressed relative to control conditions arbitrarily set to 1 (n = 2–3). Values are expressed as mean ± SEM and compared using the Dunnett's post hoc test. $^{*}P < 0.05$, $^{**}P < 0.01$, $^{***}P < 0.005$. (**G**) Screenshot of the IGV browser at the *Dpt* locus. Wy, Wy14,643. (**H**) Screenshot of the IGV browser at the *Acox1* and *Tgfb1* locus. (**I**) Screenshot of the IGV browser at the *Klf6* locus. (**J**) Relative expression of *TGFβ1* and of *Klf6*. Gene expression were measured and expressed as in **D**.

DPT is a key player in murine liver fibrogenesis. Whole body *Dpt*-deficient ($Dpt^{-/-}$) mice (30) did not exhibit major morphometric nor metabolic abnormalities compared with WT littermates, except for an increase in plasma cholesterol (Table 3). Importantly, alanine aminotransferase (ALT) and aspartate aminotransferase (AST) plasma levels, two markers of hepatic injury, and liver collagen content were normal, indicative of the absence of hepatic injury in unchallenged mice (Table 3). To investigate a functional role of DPT in liver fibrosis progression, $Dpt^{-/-}$ or $Dpt^{+/+}$ mice were next treated with CCl_4 for 4 or 7 weeks.

Table 3. Biometric and biochemical features of *Dpt*-null mice

Baseline phenotyping		
	$Dpt^{+/+}$	$Dpt^{-/-}$
Biometry		
Body mass (g)	20.28 ± 1.95	21.32 ± 1.87
Relative liver mass (%)	4.62 ± 0.49	4.81 ± 0.55
Relative kidney mass (%)	1.09 ± 0.07	1.12 ±0.08
Relative scWAT mass (%)	0.83 ± 0.23	0.64 ± 0.27
Relative pgWAT mass (%)	N/A	N/A
Relative poWAT mass (%)	1.20 ± 0.37	0.75 ± 0.22
Plasma parameters		
Cholesterol (mg/dl)	102.11 ± 14.74	128.21 ± 9.74[A]
HDL-C (mg/dl)	64.55 ± 10.98	85.30 ± 12.25[B]
TG (mg/dl)	82.73 ± 14.43	80.52 ± 11.71
AST (U/l)	125.77 ± 28.94	92.27 ± 30.31
ALT (U/l)	28.88 ± 5.81	32.61 ± 9.91
Glucose (g/l)	1.56 ± 0.18	1.69 ± 0.16
Liver content		
Cholesterol (µg/mg prot)	2.53 ± 0.17	2.69 ± 0.25
TG (µg/mg prot)	12.56 ± 3.09	13.29 ± 3.28
OH-proline (µg/g liver)	66.4 ± 5.18	73.25 ± 3.89

Data are expressed as the mean ± SEM (n = 9) and were compared using a 2-tailed t-test. [A]$P < 0.001$, [B]$P < 0.05$. N/A, not assayed; scWAT, s.c. WAT; pgWAT, perigonadal WAT; poWAT, periovarian WAT.

CCl_4 treatment did not result in differences in liver triglyceride or cholesterol content between WT and $Dpt^{-/-}$ mice after 7 weeks (D49) (Figure 4A). Plasma ALT and AST levels clearly increased in $Dpt^{+/+}$ mice in a time-dependent manner (Figure 4B). In sharp contrast, $Dpt^{-/-}$ mice were partially resistant to CCl_4-induced hepatic injury, as AST and ALT levels did not increase further after 4 weeks of treatment. Histological analysis evidenced less collagen deposition (Figure 4C) and hydroxyproline content (Figure 4C) in $Dpt^{-/-}$ livers after a 7-week exposure to CCl_4. These data therefore identify DPT as a player in oxidative stress–induced fibrosis.

We then assessed the impact of *Dpt* gene deficiency on the CCl_4-induced transcriptional response (Supplemental Table 13). The hepatic transcriptional response after 7 weeks of exposure to CCl_4 was compared between $Dpt^{-/-}$ and $Dpt^{+/+}$ mice by GSEA (Figure 5A). CCl_4 induced, in both genetic backgrounds, an inflammatory response and decreased expression of cytochrome P450 expression. However, several distinctive responses were noted. CCl_4 induced in $Dpt^{+/+}$ mice, but not in $Dpt^{-/-}$ mice, the expression of components of the integrin and Hippo signaling pathways. Accordingly, induction of the expression of the profibrotic *Ctgf* (50) was significantly lower in $Dpt^{-/-}$ mice (Figure 5B), as well as the expression of *desmin* (*Des*), a marker of HSC activation (51), and of *Cidec*, which may contribute to liver damage (52). CCl_4-treated $Dpt^{-/-}$ mice displayed an enrichment in genes of the protective *Clec7a/Dectin-1* pathway (53), indicative of macrophage skewing toward an antiinflammatory phenotype. The nuclear receptor PPARγ, which also exhibits antifibrotic activity, was also upregulated in $Dpt^{-/-}$ livers (54) (Figure 5B). Thus, loss of *Dpt* expression triggers coordinated transcriptional responses in the liver, potentially decreasing proliferative responses and ECM deposition, while favoring antiinflammatory responses. Since *Ctgf* expression is regulated by TGFβ/SMAD3 signaling (55), we further investigated whether activation of the TGFβ pathway is altered in $Dpt^{-/-}$ livers. SMAD3 and phospho-SMAD3 protein levels were significantly increased by CCl_4 treatment in $Dpt^{+/+}$ livers, but not in $Dpt^{-/-}$ livers (Figure 5C and Supplemental Figure 10). Since no alterations in *Smad3* RNA expression were observed, TGFβ responsiveness thus appears regulated by *Dpt* deficiency through posttranslational mechanisms. Such mechanisms may also implicate miRNAs, among which miR21 upregulation has been shown to enhance TGFβ-mediated pro-fibrogenic responses (56). Interestingly, CCl_4 treatment increased miR21 levels to a lesser extent in livers of $Dpt^{-/-}$ compared with $Dpt^{+/+}$ mice (Supplemental Figure 11). In contrast, levels of miR122, an abundantly expressed and functionally important hepatic miRNA (57), were unaltered. Taken together, our results are thus in line with a role for DPT to sustain activation of the TGFβ pathway as observed in skin (34, 58).

Dpt expression is downregulated upon PPARα activation in vivo. Human biopsy analysis showed that progressive fibrosis is associated with decreased PPARα expression and increased *DPT* expression (Figure 3A), whereas GABY decreases fibrosis and *Dpt* expression (Figure 3, B and C) while increasing *PPARα* expression (35). Therefore, we analyzed whether PPARα activation, which promotes NASH and fibrosis regression in rodents, could modulate *Dpt* expression.

This was first investigated in the CCl_4 model, in which liver injury is accompanied by increased expression of *Dpt* and *Col1a1*, an early marker of the fibrotic response (Figure 6, A and B). Interestingly, the induction of these genes was blunted by both elafibranor (GFT505), a mixed PPARα/δ agonist active in murine models of NASH (59) and in NASH patients (60) (Figure 6A), and fenofibrate (FF), a PPARα-specific agonist (Figure 6B). Interestingly, *Col1a1* and *Dpt* expression was already markedly increased in a diet-induced model of NASH with undetectable histological fibrosis (HF, high-sucrose, cholesterol [HF/HS/Ch]) (Figure 6C). Treatment of these mice with GFT505 also blunted the diet-induced *Col1a1* and *Dpt* expression. Finally, AAV8-mediated restoration of PPARα expression in MCDD-fed, $PPARα^{-/-}$ mice, which display enhanced but reversible NASH and fibrosis (36, 61), restored PPARα expression in the liver (Supplemental Figure 12), prevented fibrosis progression; ref. 36), and decreased *Col1a1* and *Dpt* expression

(Figure 6D). The regression of MCDD-induced fibrosis involved a transrepressive mechanism, as both WT and the DNA binding–deficient PPARα mutant (PPARαdiss) (36) repressed MCD-induced *Dpt* and *Col1a1* expression (Figure 6D). Taken together, these data indicate that PPARα interferes with *Dpt* induction both in NASH and fibrosis models.

To determine the mechanism of PPARα regulation of *Dpt* expression, we performed a survey of our own or publicly available data and found that in vivo treatment of mice with neither live bacteria, tunicamycin, IL-1, nor IL-6 (ref. 62 and data not shown) failed to induce *Dpt* expression, thereby excluding the TLR4, ER stress, NFκB, and STAT3 signaling pathways as major contributors to *Dpt* regulation. In contrast, *Dpt* expression is increased in *Pdgf-c* transgenic mice, which display chronic liver inflammation, liver injury, and fibrosis (63) in a *Tgfβ*/*Smad3*-dependent manner (64). These observations, in line with predictions based on ChIP-Seq data (Figure 2C) and our in vitro functional data (Figure 2F), point to a major role of the TGFβ signaling pathway in the regulation of *Dpt* expression.

Since PPARα has previously been reported to blunt TGFβ signaling in vascular smooth muscle cells (65), we investigated whether such a cell-autonomous process could also occur in hepatic LX2 stellate cells, which express *PPARα* and *Dpt* similarly as primary mouse HSCs (Figure 6E). PPARα activation with the selective agonist GW647 induced the expression of the canonical PPARα target gene *Cpt1* but did not influence TGFβ-induced *Dpt* expression in LX2 (Figure 6F) as well as in mouse stellate EMS404 (data not shown) cells. Furthermore, ChIP-Seq analysis of MCDD-treated, WT mouse livers treated or not with the PPARα agonist Wy14,643 did not identify any genomic binding of PPARα in the vicinity of the *DPT* gene, in contrast to the PPARα target gene *Acox1* (Figure 6, G and H). Thus, a direct genomic interference of PPARα with TGFβ-regulated transcription, as well as interference of PPARα with the TGFβ signaling pathway itself, is an unlikely mechanism for *Dpt* repression by PPARα.

Other PPARα genomic binding events were further monitored in MCDD-fed mouse liver to identify processes upstream of TGFβ signaling that are potentially targeted by PPARα (Figure 6, H and I). The region encompassing the *Tgfb1* gene, as well as that of the *Klf6* locus, displayed modest but detectable increase in density of PPARα within their coding regions, indicating a possible control by PPARα of their expression. This hypothesis was confirmed in PPARα-restored mouse liver, in which MCDD feeding increased the expression of both *Tgfβ1* and *Klf6*, a known transactivator of the *Tgfβ1* gene (66, 67) and which are repressed upon PPARα or PPARαdiss activation (Figure 6J). Taken together, these data suggest that PPARα controls *Tgfβ1* expression, most likely in hepatocytes, through direct or indirect mechanisms that remain to be fully explored.

Discussion

Monitoring gene expression changes at graded stages of the disease is a sensitive method to identify cellular processes leading to pathological states. Moreover, NASH and fibrosis reversibility suggests that at least part of the transcriptomic alterations are also reversible, allowing to identify gene products that are potentially causative of the pathological process. Unsupervised hierarchical clustering of our gene expression data did not allow a clear-cut identification of patient categories. This has already been observed in other studies (22, 24, 26), a pitfall probably relating to interindividual heterogeneity of the disease and the adaptive nature of the pathological response likely to trigger subtle changes in gene expression. Cohort stratification on the basis of metabolic parameters also did not identify massively dysregulated pathways. In contrast, a histologically based stratification, hence reflecting NAFLD severity, identified clusters of genes with specific functions in inflammation and ECM homeostasis. As a gene-by-gene comparison of transcriptomic studies of human NAFLD biopsies (our study and refs. 22, 24, 26, 27) revealed only a few overlapping genes, likely to result from different threshold and statistical tests applied to each study, we undertook a meta-analysis of available microarray datasets on histologically graded samples, although we were aware that such an approach also suffers from methodological biases such as nonstandardized tissue sampling, handling, and histological characterization and cross-platform variability. Our meta-analysis isolated 48 upregulated genes that we propose as a human NASH and fibrosis core gene signature (Supplemental Figure 6). Remarkably, GO term enrichment pointed mainly to wound-healing processes and ECM organization as the predominantly dysregulated biological processes in progression toward fibrosis, in agreement with most of the literature.

This refined analysis was made possible due to specific features of our cohort. As obesity is a risk factor for NAFLD, our cohort was derived from an obesity clinic program in which patients are prospectively screened for NAFLD. Although selecting for obese patients may introduce a bias in our study, the resulting cohort

encompasses the whole spectrum of NAFLD, including patients that ultimately appear free of NAFLD and could serve as an internal control group, in contrast to tertiary hepatology clinic patient cohorts. Known diabetics were not included, as preexisting diabetes and its treatment(s), often long-standing, could have had an important impact on disease severity at baseline and hence represent major confounders. Patients who were diagnosed with diabetes upon inclusion in the program — and hence de novo diabetics — were, however, included. Although the screening-based selection of patients and the inclusion of de novo diabetics argue for the general applicability of our results, a confirmation in other types of cohorts is obviously warranted.

The assessment of causal involvement of gene products and/or pathways in pathology cannot be made from cross-sectional analysis and is difficult to evaluate in patients outside the setting of specific pharmacological intervention studies. The paired biopsy analysis presented here was restricted to patients who underwent GABY, as it caused the most pronounced improvement (Figure 1B; ref. 16), in contrast to a weight -management program during which only a few patients achieved substantial improvement and resolution of NASH. This paired analysis, restricted to the liver and purely based on liver histology, identified genes whose dysregulated expression at specific stages of NAFLD was restored after GABY. As GABY induces specific alterations that contribute to its effect beyond what is attributable to weight loss, we propose that the observed changes in gene expression are mainly related to the histological improvement and not to the surgical procedure per se. We also estimate that our approach is the closest one can get in addressing the causal relationship between gene dysregulation and disease progression in NASH patients outside of the setting of a drug intervention trial.

An interspecies comparison further restricted the identified gene list to 34 up- and 8 downregulated genes, 16 being sensitive to GABY. GO analysis and identification of putative regulatory pathways narrowed our search to PPAR-, TGFβ-, or YAP/Hippo-dependent processes in HSCs. DPT was identified as an potential novel component of the liver fibrotic response that is specifically expressed in HSC (Figure 2; refs. 42, 43). Our combined analysis, as well as a more limited study (68), demonstrated *DPT* upregulation in the liver of NASH patients. This finding was not confirmed in a recent cross-species transcriptomic study, which relied on a cohort stratification based on the composite NAS score; this score does not isolate the fibrosis component of the disease (69) and therefore precludes the detection of altered *Dpt* expression (Supplemental Figure 9). In order to gain further insight in the potential novel role of DPT suggested by the human gene expression data analysis, further studies were conducted in preclinical models.

Phenotyping of *Dpt*-null mice did not evidence gross metabolic alterations. Previous studies suggested a role for DPT in skin wound healing and ECM maturation (70, 71). Strikingly, DPT deficiency protected the liver from increased collagen deposition in the CCl_4-induced fibrosis model (Figure 4), similar as in cutaneous fibrosis (30, 58). The hepatic transcriptional response to CCl_4 was impacted by Dpt deficiency. Whereas many HSC activation markers were still significantly increased in $Dpt^{-/-}$ livers, GSEA and gene-by-gene analysis revealed that the pro-fibrotic Hippo pathway and its target gene *Ctgf* were less activated in $Dpt^{-/-}$ livers. In addition, increased expression of the alternatively activated macrophage marker Clec7a, of the elastase Mmp12, and of PPARγ — all of them reportedly protective against fibrosis — was detected in $Dpt^{-/-}$ mouse liver. DPT therefore likely plays a role in signal transduction, as its cell-specific expression in HSC, a major contributor to fibrogenesis, results in increased ECM deposition, hence altering cell-to-cell communication. DPT interacts with decorin, which influences collagen fibrillogenesis, and increases TGFβ signaling (34). Globally increased SMAD3 activation was observed in $Dpt^{-/-}$ livers, accompanied by increased SMAD3 protein steady state levels. Taken together, these data suggest that *Dpt* deficiency interferes with signal transduction pathways involved in pro-fibrotic responses. While these conclusions are based on the use of a whole body *Dpt*-KO model, and therefore may imply indirect contributions of other Dpt-expressing organs, it is worth noting that CCl_4-induced damages are liver specific, as they stem from the conversion of CCl_4 to the $^{\cdot}CCl3$ radical by CypP450 2E1, which is exclusively expressed in the centrilobular region of the liver (72).

The regulation of *Dpt* gene expression is poorly characterized. *Dpt* promoter hypermethylation correlates with decreased *DPT* expression in human hepatocarcinoma (73), and vitamin D or glucocorticoid receptor activation increases *DPT* expression in human BM mesenchymal stem cells (74, 75). PPARα/NR1C1 is a nuclear receptor whose activation results in the normalization of atherogenic dyslipidemia. This effect is due to the transcriptional control of PPARα target genes involved in fatty acid and lipoprotein metabolism (18). The mechanisms of antiinflammatory and antifibrotic actions of PPARα are distinct from its metabolic functions and are usually considered to result from a cell autonomous, transrepressive mechanism (36).

Increased *Dpt* expression in fibrotic conditions was repressed by WT PPARα and the DNA binding–crippled PPARαdiss mutant, indicating that PPARα represses *Dpt* expression through a transrepressive mechanism. Transcriptomic and PPARα cistrome analysis converged to demonstrate that PPARα acts, at least in part, by decreasing the expression of *Klf6*, a *Tgfβ1* gene transactivator, and of *Tgfβ1* itself, but not by interfering with the TGFβ signaling pathway. This contrasts with the cell-autonomous transrepression of NFκB-activated genes by PPARα in multiple systems (18), suggesting that beneficial antiinflammatory and antifibrotic activities of PPARα agonists stem from cell-specific effects in the fibrotic liver and whose mechanisms and sites of action remain to be identified.

Transcriptomic exploration of several subtypes of NAFLD from normal liver to cirrhosis, instead of the usual dichotomous approach, combined with a meta-analysis of our and other datasets allowed the definition of a molecular signature of NASH + fibrosis. This molecular signature evolved concomitantly with the regression of histological injuries after GABY, suggesting that they are potential players in NAFLD pathophysiology and hence targets for pharmacological therapy. Further identification of DPT's role in mouse fibrosis and of its regulation by PPARα ligands active in human pathology validates our approach and provides further grounds to investigate mechanisms at play in human NAFLD.

Methods

Patients

The metabolic work-up is described in detail in the Supplemental Materials section.

Human liver biopsies

Biopsies were collected from overweight individuals visiting the Obesity Clinic at the Antwerp University Hospital as reported previously (76). Patients who presented at the clinic for a problem of overweight/obesity were prospectively screened for the presence of NAFLD and, if suspected (based on preset criteria relying on abnormal blood biochemistry assays [ALT, AST, γ glutamyl-transferase (γGT)] or ultrasound features), were offered a liver biopsy. Exclusion criteria were alcohol consumption, previous BarSur, liver diseases other than NAFLD, and lipid-lowering treatments. Patients with diagnosed diabetes were not included, as diabetes and its associated treatments were considered as major confounding factors that might have influenced the course of the disease before entering the program. Patients who were de novo diagnosed with diabetes at the baseline work-up were, however, included. Patients afterward entered a weight-management program, and some subsequently underwent GABY. A liver biopsy was repeated after 1 year of follow-up, if the patient consented (35).

Histological scoring of human liver biopsies

All biopsies were stained (H&E stain, Sirius red stain, reticulin stain, Perl's iron stain) and blind-scored by two experienced pathologists. The different histological features of NAFLD were assessed using the NASH Clinical Research Network (NASH CRN) Scoring System as described previously (35).

RNA extraction and quantitative PCR

RNA extraction, purification, and processing were described previously (35). Quantification and purity of RNA were assessed using a Nanodrop device (Nanodrop Technologies, Thermo Scientific). RNA was reverse-transcribed using the High-Capacity cDNA archive kit (Applied Biosystems) following the manufacturer's recommendations. mRNAs were analyzed using the SYBR green Brilliant II fast kit (Agilent Technologies) on an Mx3005p apparatus (Agilent Technologies). mRNA levels were normalized to the 36B4 gene level, and the fold induction was calculated using the cycle threshold (ΔΔCT) method (77).

Microarray analysis

Transcriptome analysis with Affymetrix GeneChip arrays (HuGene 2.0 ST or MoGene 2.0 ST) was performed as described (36). All liquid handling steps were performed by a GeneChip Fluidics Station 450, and GeneChips were scanned with a GeneChip Scanner 3000-7G (Affymetrix) using Command Console v4.1.2. Quality controls were performed using the Affymetrix expression console. Proprietary .CEL files were imported into Genespring (v13.1.1, Agilent Technologies) and analyzed to identify dysregulated gene patterns as described below.

Total RNA was extracted from liver biopsies. Single-stranded cDNA was prepared from 100 to 300 ng of total RNA with the GeneChip WT PLUS Reagent Kit (Affymetrix). After end-labeling and hybridization, signals were collected and normalized by the robust multiarray average (RMA) method, and the baseline was adjusted to the median of all samples (n = 87). The 5% lowest-expressed genes were filtered out, thereby identifying 37,500 entities (out of 44,629) displaying a detectable expression. A gene-level dataset was created on which quantile normalization was applied. A gene set was created that excluded all nonprotein-encoding genes and those displaying no or low variation (FC < 1.2) in expression values. This generated a 6,925-gene list coding for mRNAs with known functions (Supplemental Table 1) against which all further analysis was performed. SOM clustering was performed with a squared Euclidean distance metric and 1,500 iterations allowing for 10 gene clusters to be identified. Figures were exported from Genespring as .TIF files and processed using Corel Photopaint X3 and CorelDraw X3.

Functional annotation of identified gene clusters was carried out using the DAVID (78) and the Metascape (79) web portals. Term enrichment was obtained from the Online Mendelian Inheritance in Man (OMIM), Protein Information Resource (PIR), GO, Biocarta and Kyoto Encyclopedia of Genes and Genomes (KEGG) databases. Other human datasets were imported from the GEO repository (GSE GSE48452, GSE49541; refs. 24, 27) and processed as in house-generated data. Mouse transcriptomics data were imported from the GEO GSE73985 dataset (HFD/CCl4-treated mice) and from the GEO GSE35961 dataset (HFD/MCDD-fed mice; ref. 80).

Animal experimentation and biochemical and histological analyses

CCl_4-induced fibrosis in Dpt-KO mice. A pilot scale experiment was carried out in which 10- to 12-week-old female *Dpt*-null mice (Riken BRC; ref. 30) (n = 3) and their WT littermates (n = 4) were s.c. injected for 6 weeks by CCl_4 (Sigma-Aldrich, 0.1 ml/kg of a 1% solution in sterile olive oil, twice a week). Livers were harvested 24 hours after the last injection. Fibrosis was histologically quantified (Sirius red staining), and $Dpt^{-/-}$ livers showed an approximately 70% lower collagen deposition after CCl_4 treatment when compared with $Dpt^{+/+}$ livers. A power calculation using this size of the effect and an estimated SD of 40% for a P value < 0.05 yielded a sample size of 7 (G*Power, University of Dusseldorf, Dusseldorf, Germany; ref. 81).

The full-scale CCl_4 experiment was thus performed in 10- to 12-week-old female *Dpt*-null mice (n = 13) and their WT littermates (n = 9). Mice (~25 g) were treated 3 times a week with 0.1 ml/kg of a 2% CCl_4 solution for 1 week, then 4% (week 2), 5% (week 3), 6% (week 4), and 8% (week 5-8). Livers were harvested 24 hours after the last injection.

CCl_4-induced fibrosis in C57Bl/6J mice. C57Bl/6J mice (Charles River Laboratories) were fed a CD diet and exposed or not to CCl_4 for 3 weeks (with 0.2 ml/kg/day) 3 times a week (n = 8–12). GFT505 or fenofibrate were incorporated in the diet to achieve a 10 mpk/day or a 200 mpk/day dosage, respectively. Livers were harvested 48 hours after the last injection.

HF/HS/Ch. C57Bl/6J mice were fed either a CD or a HF/HS/Ch diet with 36% fat, 43.2% sucrose, and 0.5% cholesterol for 27 weeks (n = 9–12). GFT505 was incorporated in the diet to achieve a 10 mpk/day dosage.

MCDD. The MCDD or a CD was administered for 28 days to AAV-TBG-EGFP– or AAV-TBG-PPARα–injected PPARα-deficient mice. The synthetic PPARα agonist Wy14,643 was incorporated in the diet (0.2%) (36).

Transcript profiling. The microarray dataset is available at GEO GSE83452.

Biochemical and histological assays

Mice were weighed, and food was removed. Blood samples were taken after a 4-hour fasting by retro-orbital sinus punction under isoflurane anesthesia for free fatty acid, cholesterol, triglyceride, ALT, and AST assays (36). Mice were euthanized by cervical dislocation, and livers were weighed. The median lobes were fixed in 4% formaldehyde and embedded in paraffin for histological analysis, and remaining lobes were snap-frozen in liquid nitrogen for further analysis. Fibrosis assessment was carried out by staining liver sections with a 0.1% solution of Sirius red in 1.3% saturated aqueous picric acid solution (Sigma-Aldrich). Ten to 15 microscopic fields of each liver section were randomly chosen and microscopically photographed at a 150-fold magnification. The area occupied by collagen was quantitated by morphometry using ImageJ and expressed as a percentage of total cross-sectional area. The hydroxyproline assay was performed on 50 mg of liver, which was hydrolyzed in 6 M HCl and processed for the colorimetric assay according to the manufacturer's instructions (Quickzyme Biosciences).

Electrophoresis and Western blotting

Proteins (100 μg) from liver extracts were separated by 10% SDS-PAGE and blotted onto a PVDF membrane (Hybond-P, GE Healthcare). Anti-PPARα (sc-9000, Santa Cruz Biotechnology), anti–β-actin (sc-1616, Santa Cruz Biotechnology), anti–phospho-SMAD3 (ab52903, Abcam), and anti-SMAD3 (ab40854, Abcam) were used.

Statistics

All data were analyzed using the GraphPad Prism 6 software (GraphPad Software Inc.) or the Genespring 14.3 software (Agilent Technologies). Statistical analysis parameters are indicated in the legend to figures; $P < 0.05$ was generally considered as significant

Study approval

The human study protocol is part of the Hepadip protocol (Belgian registration number B30020071389) and approved by the Ethical Committee of the Antwerp University Hospital (file 6/25/125). Mouse experimental protocols were approved by the Lille Pasteur Institute ethical committee and carried out in agreement with European Union (EEC no. 07430) and French ethical guidelines.

Author contribution

PL analyzed genomic data. CG, BD, and HD performed microarray analysis, FL, MP, EB, and NH performed in vivo experiments and associated biochemical analysis. JV performed histological analysis of mouse livers. FPZ, EW, and MBG performed in vitro experiments. AD, GH, LV, WJK, PM, and TV collected human biopsies and histological and biochemical data. CM and JE contributed to genomic analysis. LVG, AV, and SF supervised human biopsies collection and analysis. PL, SF, and BS conceived the study, interpreted data, and wrote the manuscript, and they share the corresponding authorship. SF and BS share the senior authorship.

Acknowledgments

We thank Julie Dubois-Chevalier for help with ChIP-Seq data analysis. This study was supported by grants from the European Union (FP6 Hepadip FP6-018734 and FP7 Resolve, FP7-305707), Fondation de France (grant 2014 00047965), Fondation pour la Recherche Médicale (Equipe labellisée, DEQ20150331724), and Agence Nationale pour la Recherche (ANR-10-LBEX-46). MP is supported by Foundation for Polish Science and National Science Centre, Poland (2014/15/D/NZ5/03421).

Address correspondence to : Bart Staels, 1 rue du Pr Calmette, Institut Pasteur Lille, 59000 Lille, France. Phone: 33.320877388; Email: bart.staels@pasteur-lille.fr. Or to: Philippe Lefebvre, Building J&K, Boulevard du Pr Leclerc, 59000 Lille, France. Phone: 33.320974220; Email: philippe-claude.lefebvre@inserm.fr. Or to: Sven Francque, UZA, Wilrijkstraat 10, B-2650 Edegem, Belgium. Phone: 32.38214572; Email: sven.Francque@uza.be.

MP's current address is: International Institute of Molecular and Cell Biology, Warsaw, Poland.

1. Byrne CD, Targher G. NAFLD: a multisystem disease. *J Hepatol*. 2015;62(1 Suppl):S47–S64.
2. Satapathy SK, Sanyal AJ. Epidemiology and Natural History of Nonalcoholic Fatty Liver Disease. *Semin Liver Dis*. 2015;35(3):221–235.
3. Ekstedt M, et al. Fibrosis stage is the strongest predictor for disease-specific mortality in NAFLD after up to 33 years of follow-up. *Hepatology*. 2015;61(5):1547–1554.
4. Ellis EL, Mann DA. Clinical evidence for the regression of liver fibrosis. *J Hepatol*. 2012;56(5):1171–1180.
5. Karsdal MA, et al. Novel insights into the function and dynamics of extracellular matrix in liver fibrosis. *Am J Physiol Gastrointest Liver Physiol*. 2015;308(10):G807–G830.
6. Cox TR, Erler JT. Remodeling and homeostasis of the extracellular matrix: implications for fibrotic diseases and cancer. *Dis Model Mech*. 2011;4(2):165–178.
7. Mannaerts I, et al. The Hippo pathway effector YAP controls mouse hepatic stellate cell activation. *J Hepatol*. 2015;63(3):679–688.
8. Marrone G, Shah VH, Gracia-Sancho J. Sinusoidal communication in liver fibrosis and regeneration. *J Hepatol*. 2016;65(3):608–617.
9. Lee YA, Wallace MC, Friedman SL. Pathobiology of liver fibrosis: a translational success story. *Gut*. 2015;64(5):830–841.
10. Adams LA, et al. The natural history of nonalcoholic fatty liver disease: a population-based cohort study. *Gastroenterology*. 2005;129(1):113–121.

11. Matteoni CA, Younossi ZM, Gramlich T, Boparai N, Liu YC, McCullough AJ. Nonalcoholic fatty liver disease: a spectrum of clinical and pathological severity. *Gastroenterology*. 1999;116(6):1413–1419.
12. Vilar-Gomez E, et al. Weight Loss Through Lifestyle Modification Significantly Reduces Features of Nonalcoholic Steatohepatitis. *Gastroenterology*. 2015;149(2):367–378.e5; quiz e14.
13. Dixon JB, Bhathal PS, Hughes NR, O'Brien PE. Nonalcoholic fatty liver disease: Improvement in liver histological analysis with weight loss. *Hepatology*. 2004;39(6):1647–1654.
14. Petersen KF, Dufour S, Befroy D, Lehrke M, Hendler RE, Shulman GI. Reversal of nonalcoholic hepatic steatosis, hepatic insulin resistance, and hyperglycemia by moderate weight reduction in patients with type 2 diabetes. *Diabetes*. 2005;54(3):603–608.
15. Mathurin P, et al. Prospective study of the long-term effects of bariatric surgery on liver injury in patients without advanced disease. *Gastroenterology*. 2009;137(2):532–540.
16. Lassailly G, et al. Bariatric Surgery Reduces Features of Nonalcoholic Steatohepatitis in Morbidly Obese Patients. *Gastroenterology*. 2015;149(2):379–388.
17. Sasaki A, et al. Bariatric surgery and non-alcoholic Fatty liver disease: current and potential future treatments. *Front Endocrinol (Lausanne)*. 2014;5:164.
18. Pawlak M, Lefebvre P, Staels B. Molecular mechanism of PPARα action and its impact on lipid metabolism, inflammation and fibrosis in non-alcoholic fatty liver disease. *J Hepatol*. 2015;62(3):720–733.
19. Dubois V, Eeckhoute J, Lefebvre P, Staels B. Distinct but complementary contributions of PPAR isotypes to energy homeostasis. *J Clin Invest*. 2017;127(4):1202–1214.
20. Wree A, Broderick L, Canbay A, Hoffman HM, Feldstein AE. From NAFLD to NASH to cirrhosis-new insights into disease mechanisms. *Nat Rev Gastroenterol Hepatol*. 2013;10(11):627–636.
21. Haas JT, Francque S, Staels B. Pathophysiology and Mechanisms of Nonalcoholic Fatty Liver Disease. *Annu Rev Physiol*. 2016;78:181–205.
22. Starmann J, et al. Gene expression profiling unravels cancer-related hepatic molecular signatures in steatohepatitis but not in steatosis. *PLoS One*. 2012;7(10):e46584.
23. Yoneda M, et al. Gene expression profiling of non-alcoholic steatohepatitis using gene set enrichment analysis. *Hepatol Res*. 2008;38(12):1204–1212.
24. Arendt BM, et al. Altered hepatic gene expression in nonalcoholic fatty liver disease is associated with lower hepatic n-3 and n-6 polyunsaturated fatty acids. *Hepatology*. 2015;61(5):1565–1578.
25. Clarke JD, et al. Characterization of hepatocellular carcinoma related genes and metabolites in human nonalcoholic fatty liver disease. *Dig Dis Sci*. 2014;59(2):365–374.
26. Lake AD, et al. Analysis of global and absorption, distribution, metabolism, and elimination gene expression in the progressive stages of human nonalcoholic fatty liver disease. *Drug Metab Dispos*. 2011;39(10):1954–1960.
27. Moylan CA, et al. Hepatic gene expression profiles differentiate presymptomatic patients with mild versus severe nonalcoholic fatty liver disease. *Hepatology*. 2014;59(2):471–482.
28. Murphy SK, et al. Relationship between methylome and transcriptome in patients with nonalcoholic fatty liver disease. *Gastroenterology*. 2013;145(5):1076–1087.
29. Dudley JT, Tibshirani R, Deshpande T, Butte AJ. Disease signatures are robust across tissues and experiments. *Mol Syst Biol*. 2009;5:307.
30. Takeda U, et al. Targeted disruption of dermatopontin causes abnormal collagen fibrillogenesis. *J Invest Dermatol*. 2002;119(3):678–683.
31. Wu W, et al. Dermatopontin regulates fibrin formation and its biological activity. *J Invest Dermatol*. 2014;134(1):256–263.
32. Wu W, et al. Functional peptide of dermatopontin produces fibrinogen fibrils and modifies its biological activity. *J Dermatol Sci*. 2014;76(1):34–43.
33. Kato A, et al. Identification of fibronectin binding sites in dermatopontin and their biological function. *J Dermatol Sci*. 2014;76(1):51–59.
34. Okamoto O, Fujiwara S, Abe M, Sato Y. Dermatopontin interacts with transforming growth factor beta and enhances its biological activity. *Biochem J*. 1999;337 (Pt 3):537–541.
35. Francque S, et al. PPARα gene expression correlates with severity and histological treatment response in patients with non-alcoholic steatohepatitis. *J Hepatol*. 2015;63(1):164–173.
36. Pawlak M, et al. The transrepressive activity of peroxisome proliferator-activated receptor alpha is necessary and sufficient to prevent liver fibrosis in mice. *Hepatology*. 2014;60(5):1593–1606.
37. Levene AP, Goldin RD. The epidemiology, pathogenesis and histopathology of fatty liver disease. *Histopathology*. 2012;61(2):141–152.
38. Takahashi Y, Soejima Y, Fukusato T. Animal models of nonalcoholic fatty liver disease/nonalcoholic steatohepatitis. *World J Gastroenterol*. 2012;18(19):2300–2308.
39. Wong FW, Chan WY, Lee SS. Resistance to carbon tetrachloride-induced hepatotoxicity in mice which lack CYP2E1 expression. *Toxicol Appl Pharmacol*. 1998;153(1):109–118.
40. Braeuning A, et al. Differential gene expression in periportal and perivenous mouse hepatocytes. *FEBS J*. 2006;273(22):5051–5061.
41. Seki E, Schwabe RF. Hepatic inflammation and fibrosis: functional links and key pathways. *Hepatology*. 2015;61(3):1066–1079.
42. Azimifar SB, Nagaraj N, Cox J, Mann M. Cell-type-resolved quantitative proteomics of murine liver. *Cell Metab*. 2014;20(6):1076–1087.
43. Ding C, et al. A Cell-type-resolved Liver Proteome. *Mol Cell Proteomics*. 2016;15(10):3190–3202.
44. Milani S, et al. Undulin RNA and protein expression in normal and fibrotic human liver. *Hepatology*. 1994;20(4 Pt 1):908–916.
45. Arriazu E, et al. Extracellular matrix and liver disease. *Antioxid Redox Signal*. 2014;21(7):1078–1097.
46. Neill T, Schaefer L, Iozzo RV. Instructive roles of extracellular matrix on autophagy. *Am J Pathol*. 2014;184(8):2146–2153.
47. Krishnan A, et al. Lumican, an extracellular matrix proteoglycan, is a novel requisite for hepatic fibrosis. *Lab Invest*. 2012;92(12):1712–1725.
48. Kato A, et al. Dermatopontin interacts with fibronectin, promotes fibronectin fibril formation, and enhances cell adhesion. *J Biol*

Chem. 2011;286(17):14861–14869.
49. Mederacke I, et al. Fate tracing reveals hepatic stellate cells as dominant contributors to liver fibrosis independent of its aetiology. *Nat Commun*. 2013;4:2823.
50. Huang G, Brigstock DR. Regulation of hepatic stellate cells by connective tissue growth factor. *Front Biosci (Landmark Ed)*. 2012;17:2495–2507.
51. Fujii T, et al. Mouse model of carbon tetrachloride induced liver fibrosis: Histopathological changes and expression of CD133 and epidermal growth factor. *BMC Gastroenterol*. 2010;10:79.
52. Xu MJ, et al. Fat-Specific Protein 27/CIDEC Promotes Development of Alcoholic Steatohepatitis in Mice and Humans. *Gastroenterology*. 2015;149(4):1030–41.e6.
53. Seifert L, et al. Dectin-1 Regulates Hepatic Fibrosis and Hepatocarcinogenesis by Suppressing TLR4 Signaling Pathways. *Cell Rep*. 2015;13(9):1909–1921.
54. Morán-Salvador E, et al. Cell-specific PPARγ deficiency establishes anti-inflammatory and anti-fibrogenic properties for this nuclear receptor in non-parenchymal liver cells. *J Hepatol*. 2013;59(5):1045–1053.
55. Liu Y, et al. Transforming growth factor-β (TGF-β)-mediated connective tissue growth factor (CTGF) expression in hepatic stellate cells requires Stat3 signaling activation. *J Biol Chem*. 2013;288(42):30708–30719.
56. Dattaroy D, et al. Micro-RNA 21 inhibition of SMAD7 enhances fibrogenesis via leptin-mediated NADPH oxidase in experimental and human nonalcoholic steatohepatitis. *Am J Physiol Gastrointest Liver Physiol*. 2015;308(4):G298–G312.
57. Hu J, Xu Y, Hao J, Wang S, Li C, Meng S. MiR-122 in hepatic function and liver diseases. *Protein Cell*. 2012;3(5):364–371.
58. Okamoto O, Suzuki Y, Kimura S, Shinkai H. Extracellular matrix 22-kDa protein interacts with decorin core protein and is expressed in cutaneous fibrosis. *J Biochem*. 1996;119(1):106–114.
59. Staels B, et al. Hepatoprotective effects of the dual peroxisome proliferator-activated receptor alpha/delta agonist, GFT505, in rodent models of nonalcoholic fatty liver disease/nonalcoholic steatohepatitis. *Hepatology*. 2013;58(6):1941–1952.
60. Ratziu V, et al. Elafibranor, an Agonist of the Peroxisome Proliferator-Activated Receptor-α and -δ, Induces Resolution of Nonalcoholic Steatohepatitis Without Fibrosis Worsening. *Gastroenterology*. 2016;150(5):1147–1159.e5.
61. Machado MV, et al. Mouse models of diet-induced nonalcoholic steatohepatitis reproduce the heterogeneity of the human disease. *PLoS One*. 2015;10(5):e0127991.
62. Ramadoss P, Chiappini F, Bilban M, Hollenberg AN. Regulation of hepatic six transmembrane epithelial antigen of prostate 4 (STEAP4) expression by STAT3 and CCAAT/enhancer-binding protein alpha. *J Biol Chem*. 2010;285(22):16453–16466.
63. Wright JH, et al. Paracrine activation of hepatic stellate cells in platelet-derived growth factor C transgenic mice: evidence for stromal induction of hepatocellular carcinoma. *Int J Cancer*. 2014;134(4):778–788.
64. Lee JI, et al. Role of Smad3 in platelet-derived growth factor-C-induced liver fibrosis. *Am J Physiol, Cell Physiol*. 2016;310(6):C436–C445.
65. Kintscher U, et al. PPARalpha inhibits TGF-beta-induced beta5 integrin transcription in vascular smooth muscle cells by interacting with Smad4. *Circ Res*. 2002;91(11):e35–e44.
66. Stärkel P, et al. Oxidative stress, KLF6 and transforming growth factor-beta up-regulation differentiate non-alcoholic steatohepatitis progressing to fibrosis from uncomplicated steatosis in rats. *J Hepatol*. 2003;39(4):538–546.
67. Kim Y, et al. Transcriptional activation of transforming growth factor beta1 and its receptors by the Kruppel-like factor Zf9/core promoter-binding protein and Sp1. Potential mechanisms for autocrine fibrogenesis in response to injury. *J Biol Chem*. 1998;273(50):33750–33758.
68. Baker SS, Baker RD, Liu W, Nowak NJ, Zhu L. Role of alcohol metabolism in non-alcoholic steatohepatitis. *PLoS One*. 2010;5(3):e9570.
69. Teufel A, et al. Comparison of Gene Expression Patterns Between Mouse Models of Nonalcoholic Fatty Liver Disease and Liver Tissues From Patients. *Gastroenterology*. 2016;151(3):513–525.e0.
70. Tracy LE, Minasian RA, Caterson EJ. Extracellular Matrix and Dermal Fibroblast Function in the Healing Wound. *Adv Wound Care (New Rochelle)*. 2016;5(3):119–136.
71. Okamoto O, Fujiwara S. Dermatopontin, a novel player in the biology of the extracellular matrix. *Connect Tissue Res*. 2006;47(4):177–189.
72. Koop DR. Oxidative and reductive metabolism by cytochrome P450 2E1. *FASEB J*. 1992;6(2):724–730.
73. Fu Y, et al. DNA methylation-mediated silencing of matricellular protein dermatopontin promotes hepatocellular carcinoma metastasis by α3β1 integrin-Rho GTPase signaling. *Oncotarget*. 2014;5(16):6701–6715.
74. Pochampally RR, Ylostalo J, Penfornis P, Matz RR, Smith JR, Prockop DJ. Histamine receptor H1 and dermatopontin: new downstream targets of the vitamin D receptor. *J Bone Miner Res*. 2007;22(9):1338–1349.
75. Derfoul A, Perkins GL, Hall DJ, Tuan RS. Glucocorticoids promote chondrogenic differentiation of adult human mesenchymal stem cells by enhancing expression of cartilage extracellular matrix genes. *Stem Cells*. 2006;24(6):1487–1495.
76. Verrijken A, et al. Prothrombotic factors in histologically proven nonalcoholic fatty liver disease and nonalcoholic steatohepatitis. *Hepatology*. 2014;59(1):121–129.
77. Schmittgen TD, Livak KJ. Analyzing real-time PCR data by the comparative C(T) method. *Nat Protoc*. 2008;3(6):1101–1108.
78. Dennis G, et al. DAVID: Database for Annotation, Visualization, and Integrated Discovery. *Genome Biol*. 2003;4(5):P3.
79. Tripathi S, et al. Meta- and Orthogonal Integration of Influenza "OMICs" Data Defines a Role for UBR4 in Virus Budding. *Cell Host Microbe*. 2015;18(6):723–735.
80. Kita Y, et al. Metformin prevents and reverses inflammation in a non-diabetic mouse model of nonalcoholic steatohepatitis. *PLoS One*. 2012;7(9):e43056.
81. Faul F, Erdfelder E, Buchner A, Lang AG. Statistical power analyses using G*Power 3.1: tests for correlation and regression analyses. *Behav Res Methods*. 2009;41(4):1149–1160.
82. Chen EY, et al. Enrichr: interactive and collaborative HTML5 gene list enrichment analysis tool. *BMC Bioinformatics*. 2013;14:128.
83. Kuleshov MV, et al. Enrichr: a comprehensive gene set enrichment analysis web server 2016 update. *Nucleic Acids Res*. 2016;44(W1):W90–W97.